Mechanical link between durotaxis, cell polarity and anisotropy during cell migration

D Aubry[1], **M Gupta**[2,3], **B Ladoux**[2,3] and **R Allena**[4]

[1] Ecole Centrale Paris, Laboratoire MSSMat UMR CNRS 8579, Grande Voie des Vignes, 92295 Châtenay-Malabry, France
[2] Mechanobiology Institute, Cell adhesion and Mechanics Laboratory, T-Lab, #09-01 5 A, Engineering Drive 1, Singapore 11741
[3] Institut Jacques Monod, Cell adhesion and Mechanics Laboratory UMR CNRS 7592, 10 rue Hélène Brion, 75205 Paris Cedex 13, France
[4] Arts et Metiers ParisTech, LBM, 151 Bd de l'hôpital, 75013 Paris, France

E-mail: rachele.allena@ensam.eu

Abstract

Cell migration, a fundamental mechanobiological process, is highly sensitive to the biochemical and mechanical properties of the environment. Efficient cell migration is ensured by the intrinsic polarity of the cell, which triggers a transition from an isotropic to an anisotropic configuration of the acto-mysion filaments responsible for the protrusion–contraction movement of the cell. Additionally, polarity may be highly influenced by the substrate rigidity, which results in a phenomenon called durotaxis. In the present work, we propose a two-dimensional finite element model able to capture three main features of cell migration: durotaxis, cell polarity and anisotropy. The cell is modelled as a continuum able to develop cyclic active strains regulated by the polymerization and depolymerization of the acto-myosin filaments and synchronized with the adhesion forces between the cell and the substrate underneath. A generalized Maxwell model is used to describe the viscoelastic behaviour of the cell constituted by a solid anisotropic branch with active strains (i.e. the acto-myosin filaments) and a fluid viscoelastic branch (i.e. the cytoplasm). Several types of substrate have been tested which are homogeneously soft or stiff or include both regions. The numerical results have been qualitatively compared with experimental observations showing a good agreement and have allowed us to find the mechanical link between durotaxis, cell polarity and anisotropy.

1. Introduction

Cell migration plays a fundamental role during several biological phenomena and it is sensitive to both the biochemical and mechanical properties of the environment. Actually, cells probe the stiffness of the extracellular matrix (ECM) by adhering to the surrounding fibres and pulling on them. Thus, ECM may be critical for many cellular functions such as adhesion [1], migration [2], differentiation [3] and polarization [4]. Among the potential candidates responsible for the cell mechanosensitivity, focal adhesion (FA) seems to be the most plausible due to the existing correlation between their surfaces and the exerted force inducing an elastic strain [5–8]. It has been shown that the ion calcium channels may be involved in the building up of the cellular tension in response to a mechanical signal [2, 9, 10]. Additionally, recent observations

[11, 12] as well as a mechanical model [13] have suggested that the acto-myosin complexes can act as global sensors of rigidity [14]. Huge efforts are continuing to be made to understand such responses and uncover the molecular details of these biomechanical pathways [15]. However, the coupling between local and global scales of the mechanical signalling modules described above is far from being understood [16]. The difficulty lies in the complexity of the mechanosensitive feedback responses that occur at various time and length scales. The most challenging problem is to identify how all these signals are integrated in order to induce a global response at the cell scale.

From a physical point of view, it is still unclear whether the mechanosensitivity is regulated by the stresses generated by the cell or by strains undergone by the ECM. Nevertheless, it is evident that

determining the mechanical principles at the basis of the forces' transmission between the cell and the ECM would allow to us explain the behavioural divergences during cellular activities within environments with different stiffness.

1.1. Cell polarity and durotaxis

Cell polarity or polarization is the ability of a cell to create and maintain an asymmetric distribution of intrinsic subdomains with distinct chemical, physical and mechanical properties. Cell polarity is relevant during migration and induces a transition from a symmetric and isotropic configuration (i.e. acto-myosin filaments radially oriented) to an asymmetric and anisotropic configuration (i.e. acto-myosin filaments oriented in the direction of migration).

Mechanical properties of the ECM and more specifically its rigidity may induce cell polarization [4, 17–19]. This results in a phenomenon called durotaxis which consists of the orientation of the acto-myosin filaments along the stiffness gradient of the ECM or along the stress fields generated by neighbour cells in order to reduce the elastic energy [4, 20, 21]. In fact, the acto-myosin filaments tend to adapt to the ECM rigidity and to develop higher traction forces on stiffer substrates [12, 22]. Such adaptation, coupled with the FA sensitivity, might explain how the ECM stiffness triggers cell polarization and migration.

During the last few years, several analytical and numerical works have been proposed in the literature to investigate durotaxis during cell migration [16, 23].

Moreo *et al* [24] proposed an extension of the Hill's model for skeletal muscle behaviour to investigate cell mechanosensing, migration and proliferation. Their results allow us to predict the cell response on elastic substrates and under different loading conditions. Dokukina and Gracheva [25] developed a 2D discrete model of a viscoelastic fibroblast cell using a Delaunay triangulation. At each node the balance of the forces is calculated as the contribution of the frictional force between the cell and the substrate, the passive viscoelastic force and the active force. The authors have evaluated the cell behaviour over a substrate with a rigidity step and their results are in agreement with specific experimental observations. In fact, they found that the cell (i) preferentially moves on stiffer substrate and (ii) turns away from the soft substrate when it approaches it as reported by [2].

In Harland *et al* [26] the cell is a collection of stress fibres undergoing contraction and the birth/death process. The formation of new fibres, whose rate depends on the substrate stiffness, is stochastic and centred at the cell centre of mass. The model shows that cells for which the adhesions slide more slowly and stress fibres form readily on stiff substrates also exhibit durotaxis. Stefanoni *et al* [27] employed Langevin equations to take into account the local mechanical properties of the substrate underneath and analyze

two distinct configurations for an isotropic and a biphasic substrate. Trichet *et al* [18] introduced a phenomenological model based on active gel theory showing that cells preferentially migrate over stiff substrates and find an optimal range of rigidity leading to efficient migration. Finally, in Allena and Aubry [28] a 2D mechanical model is proposed to simulate cell migration over an heterogeneous substrate. The cell is able to adopt two different strategies (i.e. 'run-and-tumble' and 'look-and-run' strategies) to avoid the soft regions inhibiting the adhesion.

1.2. Objective of the present work

In the present paper, we propose a 2D finite element work to simulate single cell migration over substrate with different rigidities. To do so, the model is based on the following assumptions:

(1) To take into account the durotaxis phenomenon, the underneath substrate is represented as a square which may be homogenously soft or stiff or include both types of regions. Additionally, a viscous force which inhibits the cell progression is associated to the soft domains;

(2) As in previous works [28, 29], the cell is modelled as a continuum, with initial circular shape. It is able to develop radial and cyclic active strains of protrusion and contraction, which are assumed to be regulated by the polymerization and depolymerization processes of the actin filaments, respectively. Such strains are synchronized with the adhesion forces between the cell and the substrate and exerted over the frontal and rear adhesion surfaces in the direction of migration;

(3) The direction of migration is triggered by an external attractive source [28];

(4) A generalized viscoelastic Maxwell model has been used to describe the mechanical behaviour of the cell and it includes a viscoelastic (i.e. the cytoplasm) and an anisotropic elastic (i.e. the actin filaments) branch.

The main objective of the work is to highlight the mechanical link between durotaxis and cell anisotropy and polarity and the influence of one of these aspect over the other two. The paper is organized as follows. First, the geometrical description of both the cell and the substrate is proposed. Second, the mechanical framework, the constitutive model and the active strain implementation are described. Finally, the results are presented. The cell efficiency has been evaluated in terms of covered distance, migration speed and mechanical stresses and the outcomes have been qualitatively compared to experimental observations.

2. Material and methods

2.1. Stiff and soft substrate

The underneath substrate is represented by a square. Both stiff (Ω_{stiff}) and soft (Ω_{soft}) regions are described by two characteristic functions and two configurations have been tested. First, both the stiff ($h_{\text{stiff},r}$) and the soft ($h_{\text{soft},r}$) regions are considered as rectangles separated by a sharp frontier. Therefore, the domains are defined as

$$h_{\text{stiff},r} = \begin{cases} 1 & \text{if } x < x_0 \\ 0 & \text{otherwise} \end{cases}$$
$$h_{\text{soft},r} = \begin{cases} 1 & \text{if } x > x_0 \\ 0 & \text{otherwise} \end{cases} \quad (1)$$

where x is the horizontal coordinate of any particle and x_0 is a constant value.

Second, a mapped substrate constituted by five circular stiff regions surrounded by a soft domain has been obtained and the associated characteristic functions read

$$h_{\text{stiff},c} = \begin{cases} 1 & \text{if } \sum \left(x - x_{\text{stiff},i} \right)^2 + \left(y - y_{\text{stiff},i} \right)^2 - r_{\text{st}}^2 \\ 0 & \text{otherwise} \end{cases}$$
$$h_{\text{soft},c} = 1 - h_{\text{stiff},c} \quad (2)$$

where $y, x_{\text{stiff},i}, y_{\text{stiff},i}$ and r_{stiff} are respectively the vertical coordinate of any particle and the spatial coordinates of the centres and the radius of the circular regions.

According to the substrate stiffness, a viscous force $f_{\text{substrate}}$ applies and reads

$$f_{\text{substrate}} = \begin{cases} -\mu_{\text{substrate}} v & \text{on } \Omega_{\text{soft}} \\ 0 & \text{on } \Omega_{\text{stiff}} \end{cases} \quad (3)$$

where $\mu_{\text{substrate}}$ and v are the substrate friction coefficient and the cell velocity, respectively.

2.2. Cell geometry

We consider a cell with initial shape approximated by a two-dimensional (2D) circle Ω_{cell} of radius r_{cell} (figure 1). The cell is equipped with frontal (Ω_f) and rear (Ω_r) adhesion regions, which allow the adhesion between the cell and the substrate underneath [28, 30] (figure 1(b), section A.1) and are developed in the direction of migration d. Both regions are described through two characteristic functions as follows

$$h_f(\boldsymbol{p}) = \begin{cases} 1 & \left(\boldsymbol{p} - \boldsymbol{c}_{\text{cell}}, \boldsymbol{d} \right) > l_f \\ 0 & \text{otherwise} \end{cases}$$
$$h_r(\boldsymbol{p}) = \begin{cases} 1 & \left(\boldsymbol{p} - \boldsymbol{c}_{\text{cell}}, \boldsymbol{d} \right) < - l_r \\ 0 & \text{otherwise} \end{cases} \quad (4)$$

with $d = \cos(\theta) i_x + \sin(\theta) i_y$ the direction of migration as function of the angle θ, l_f and l_r the distances of $\boldsymbol{c}_{cell}$ from the boundaries of Ω_f and Ω_r respectively (figure 1), $\boldsymbol{p} = \boldsymbol{x} - \boldsymbol{u}$ the initial position
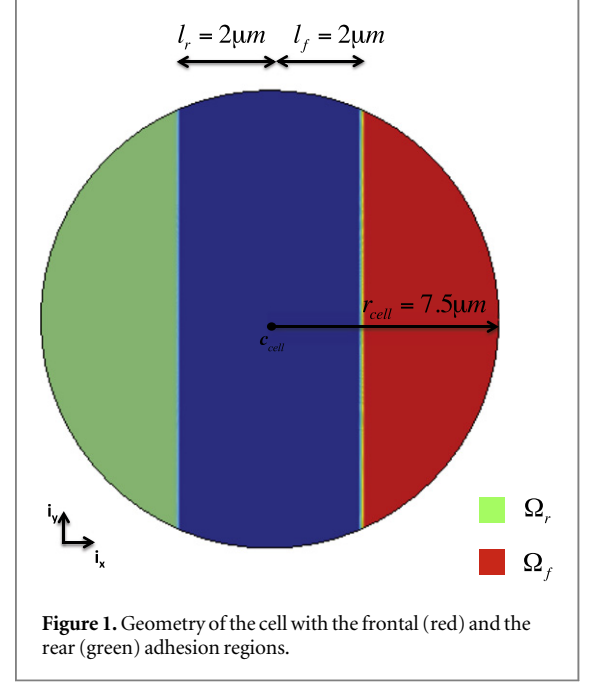

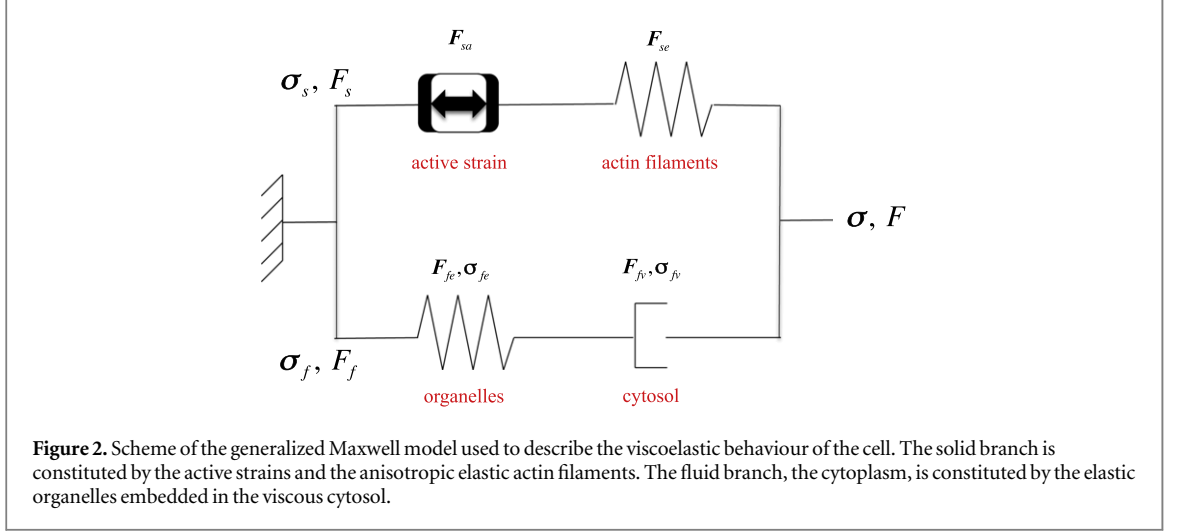**Figure 1.** Geometry of the cell with the frontal (red) and the rear (green) adhesion regions.

of any particle, where $\boldsymbol{x}$ and $\boldsymbol{u}$ are respectively the actual position and the displacement.

2.3. Mechanics and constitutive behaviour of the cell

Let ρ be the cell density, $\boldsymbol{a}$ the acceleration, σ the Cauchy stress, $\boldsymbol{F}$ the deformation gradient and J its determinant, then conservation of momentum with respect to the initial configuration in the coordinates system $\boldsymbol{p}$ is given by

$$\rho \boldsymbol{a} = \boldsymbol{Div}_{\boldsymbol{p}} \left(J \sigma \boldsymbol{F}^{-T} \right) + \boldsymbol{f}_{\text{adh}} + \boldsymbol{f}_{\text{substrate}} \quad (5)$$

where $\boldsymbol{f}_{\text{adh}}$ indicates the viscous adhesion forces between the cell and the substrate (section 2.3). Here, all the body forces but the inertial effects are neglected. In fact, it has been shown that they may play a significant role during the rapid protrusion phase [31, 32]. Additionally, from a numerical point of view, taking into account small accelerations improves the convergence performances. The cell is constituted of two main phases: a solid (i.e. the actin filaments) and a fluid (i.e. the cytoplasm) phase. Then, the actin filaments are considered rather elastic, while the cytoplasm shows a viscoelastic behaviour. Additionally, we assume that the polymerization of the actin filaments, which occurs at the frontal edge of the cell [33], is responsible of the cell protrusion, whereas their depolymerization generates the contractile stress at the rear of the cell [34]. Nevertheless, the polymerization of the actin filaments only occurs when the cell is able to adhere to the underneath substrate, whereas in the absence of adhesion the cell pulses in place [28]. In the former case, the cell acquires an elongated shape in the direction of migration $\boldsymbol{d}$, which becomes the principal axis of anisotropy. In the latter case instead, the cell radially expands and contracts in an isotropic way.

3

Figure 2. Scheme of the generalized Maxwell model used to describe the viscoelastic behaviour of the cell. The solid branch is constituted by the active strains and the anisotropic elastic actin filaments. The fluid branch, the cytoplasm, is constituted by the elastic organelles embedded in the viscous cytosol.

As in previous works [28, 30], we use a generalized Maxwell model to describe the global mechanical behaviour of the cell (figure 2). Consequently, the total Cauchy's stress $\boldsymbol{\sigma}$ is equal to

$$\boldsymbol{\sigma} = \boldsymbol{\sigma}_s + \boldsymbol{\sigma}_f \qquad (6)$$

with $\boldsymbol{\sigma}_s$ and $\boldsymbol{\sigma}_f$ the solid and the fluid Cauchy's stresses, respectively. The transformation gradient $\boldsymbol{F}$ is the same in the solid and the fluid branch, so that we can write

$$\boldsymbol{F} = \boldsymbol{D}_p \boldsymbol{u} + \boldsymbol{I} = \boldsymbol{F}_s = \boldsymbol{F}_f \qquad (7)$$

with $\boldsymbol{D}_p \boldsymbol{u} = \sum_{m=1}^{3} \frac{\partial \boldsymbol{u}}{\partial p_m} \otimes i_m$, $\boldsymbol{u}$ the displacement and $\boldsymbol{I}$ the identity matrix [35, 36].

In the solid phase (i.e. the actin filaments), $\boldsymbol{\sigma}_{se} = \boldsymbol{\sigma}_{sa}$ with se and sa standing for solid elastic and solid active respectively. Thus, we have

$$\boldsymbol{\sigma}_{se} = \frac{1}{J_{se}} \boldsymbol{F}_{se} \boldsymbol{S}_{se} \boldsymbol{F}_{se}^T \qquad (8)$$

where J_{se} is the determinant of solid elastic deformation tensor $\boldsymbol{F}_{se}$, $\boldsymbol{S}_{se}$ is the second Piola–Kirchoff solid elastic stress tensor calculated in the global system of coordinates, which is computed as an anisotropic hyperelastic Saint-Venant material as follows

$$\boldsymbol{S}_{se} = \boldsymbol{R} \boldsymbol{C}_{\mathrm{loc}} \left(\boldsymbol{R}^T \boldsymbol{E}_{se} \boldsymbol{R} \right) \boldsymbol{R}^T \qquad (9)$$

where $\boldsymbol{R}$ is the classical rotation matrix leading to $\boldsymbol{p}_{\mathrm{loc}} = \boldsymbol{R} \boldsymbol{p}$, with $\boldsymbol{p}_{\mathrm{loc}}$ the initial position in the local orthonormal system of coordinates $\left(i_\theta, i_\alpha \right)$. For the sake of clarity, we provide here the expression of the inverse of the local elastic tensor $\boldsymbol{C}_{\mathrm{loc}}^{-1}$ as

$$\boldsymbol{C}_{\mathrm{loc}}^{-1} = \sum_{\substack{m=\theta,\alpha \\ n=\theta,\alpha}} A_{mn} \left(i_m \otimes i_m \right) \otimes \left(i_n \otimes i_n \right) + B_{mn}$$
$$\times \left(i_m \otimes i_n \right) \otimes \left(i_m \otimes i_n \right) \qquad (10)$$

with A_{mn} and B_{mn} two symmetric matrices whose components are

$$A_{\theta\theta} = \frac{1}{E_\theta}$$

$$A_{\theta\alpha} = -\frac{\nu_{\theta\alpha}}{E_\theta}$$

$$A_{\alpha\theta} = -\frac{\nu_{\alpha\theta}}{E_\alpha}$$

$$A_{\alpha\alpha} = \frac{1}{E_\alpha}$$

$$B_{\theta\theta} = B_{\alpha\alpha} = 0$$
$$B_{\theta\alpha} = B_{\alpha\theta} = G_{\theta\alpha} \qquad (11)$$

with $\nu_{\theta\alpha}$ and $\nu_{\alpha\theta}$ the Poisson ratios and $G_{\theta\alpha}$ the shear modulus of the cell in the local coordinates system. The Young moduli E_θ and E_α are defined as follows

$$E_\alpha = E_\theta \quad \text{on } \Omega_{\mathrm{soft}}$$
$$E_\alpha = 0.1 E_\theta \quad \text{on } \Omega_{\mathrm{stiff}} \qquad (12)$$

The Green–Lagrange solid elastic strain tensor $\boldsymbol{E}_{se}$ is expressed as

$$\boldsymbol{E}_{se} = \frac{1}{2} \left(\boldsymbol{F}_{se}^T \boldsymbol{F}_{se} - \boldsymbol{I} \right) \qquad (13)$$

where $\boldsymbol{F}_{se}$ is given by

$$\boldsymbol{F}_{se} = \boldsymbol{F}_s \boldsymbol{F}_{sa}^{-1} \qquad (14)$$

with $\boldsymbol{F}_s$ and $\boldsymbol{F}_{sa}$ being respectively the total solid and the solid active deformation tensors. $\boldsymbol{F}_{se}$ is triggered by the interaction between the cell and the underneath substrate, whereas $\boldsymbol{F}_{sa}$ describes the cyclic and active pulsatile movement of the cell and is defined in the next section. Here, we have chosen the active strain approach since it appears to be more robust from a mathematical point of view than the active stress one [37]. Additionally, its physiological relevance has already been shown in several biological context [28, 38–41].

In the fluid phase (i.e. the cytoplasm), the deformation gradient $\boldsymbol{F}_f$ is also multiplicatively decomposed as

$$\boldsymbol{F}_f = \boldsymbol{F}_{fe} \boldsymbol{F}_{fv} \qquad (15)$$

where *fe* and *fv* stand for fluid elastic and fluid viscoelastic respectively.

The Cauchy's stress $\boldsymbol{\sigma}_f$ reads

$$\boldsymbol{\sigma}_f = 2\mu \boldsymbol{D}_{fv} \qquad (16)$$

with μ the viscosity of the cytoplasm and $\boldsymbol{D}_{f,v}$ the eulerian strain rate computed from the strain gradient velocity as follows

$$2\boldsymbol{D}_{fv} = \boldsymbol{F}_{fv}\boldsymbol{F}_{fv}^{-1} + \boldsymbol{F}_{fv}^{-T}\dot{\boldsymbol{F}}_{fv}^{T} \qquad (17)$$

2.4. Active strains and intra-synchronization

To describe the oscillating movement of the cell, some assumptions have been made.

(1) The cell is able to develop radial active strains of protrusion and contraction;

(2) As soon as the cell is able to adhere to the underneath substrate, a lamellipodium is formed at the leading edge and in the direction of migration $\boldsymbol{d}$.

Therefore, the solid active deformation tensor $\boldsymbol{F}_{sa}$ reads

$$
\boldsymbol{F}_{sa} = \begin{cases} e_{a0}\,\sin\left(2\pi\dfrac{t}{T}\right)\boldsymbol{i}_r \otimes \boldsymbol{i}_r & \text{if } \sin\left(2\pi\dfrac{t}{T}\right) > 0 \\[2mm] \dfrac{e_{a0}}{2}\,\sin\left(2\pi\dfrac{t}{T}\right)\boldsymbol{i}_r \otimes \boldsymbol{i}_r & \text{if } \sin\left(2\pi\dfrac{t}{T}\right) < 0 \end{cases} \qquad (18)
$$

where e_{a0} is the amplitude of the active strain, t is time, T is the migration period, $\otimes$ indicates the tensorial product and $\boldsymbol{i}_r$ is defined as

$$\boldsymbol{i}_r = \cos(\varphi)\boldsymbol{i}_x + \sin(\varphi)\boldsymbol{i}_y \qquad (19)$$

where $\varphi = \text{arctg}\left(\frac{y}{x}\right)$.

As numerically shown [28], in order to be able to effectively migrate, the cell must adhere on the substrate; otherwise, it would only deform in place. Thus, an intra-synchronization is required which coordinates the cyclic protrusion–contraction deformations with the adhesion forces f_{adh} (equation (5)) generated between the cell frontal and rear adhesion surfaces and the underneath substrate in the direction of migration $\boldsymbol{d}$. As in previous works [28, 30, 42, 43], such forces are assumed to be viscous and may be distinguished into a frontal ($f_{\text{adh},f}$) and a rear ($f_{\text{adh},r}$) force as follows

$$f_{\text{adh},f}(\boldsymbol{n}_{\text{cell}}) = -\mu_{\text{adh}}h_{\text{sync}}\left(-\frac{\partial \boldsymbol{F}_{sa}}{\partial t}\right)\boldsymbol{v} \quad \text{on } \Omega_f$$

$$f_{\text{adh},r}(\boldsymbol{n}_{\text{cell}}) = -\mu_{\text{adh}}h_{\text{sync}}\left(\frac{\partial \boldsymbol{F}_{sa}}{\partial t}\right)\boldsymbol{v} \quad \text{on } \Omega_r \qquad (20)$$

with $\boldsymbol{n}_{\text{cell}}$ the outward normal to the cell boundary, μ_{adh} the friction coefficient and $\boldsymbol{v}$ the cell velocity. The characteristic function h_{sync} is the key ingredient of the preceding equations since it couples the adhesion forces with the active strains, which results in the intra-synchronization mentioned above. Thus, we observe two main phases during the migratory movement of the cell: (i) the protrusion and the adhesion at the rear edge, and (ii) the contraction and the adhesion at the frontal edge.

3. Results and discussion

Simulations have been run using Comsol Multiphysics 3.5 a. At the initial time point, the cell has a circular shape centred in $\boldsymbol{c}_{\text{cell}}(0, 0)$ with radius r_{cell} equal to 7.5 μm (figure 1). The cell Young modulus E_θ is equal to 10^4 Pa [44], whereas E_α runs from 10^3 Pa to 10^4 Pa over stiff and soft substrates respectively. The Poisson's ratios $\nu_{\theta\alpha}$ and $\nu_{\alpha\theta}$ have been set to 0.3 and the shear modulus $G_{\theta\alpha}$ varies from 384 Pa to 3846 Pa respectively over soft and stiff substrates. The cell density ρ has been set to 1000 kg m^{-3} [45] and the viscous friction coefficient μ_{adh} is equal 10^8 Pa-s/m. Finally, the intensity of the active strain e_{a0} and the migration period T have been chosen equal to 0.2 and 60 s, respectively. The underneath substrate has a square shape with dimensions 70 μm $\times$ 70 μm and is centred in $(-15\,\mu\text{m}, -15\,\mu\text{m})$. All the geometrical and mechanical parameters of the model have been reported in table 1.

3.1. Soft versus stiff substrates

For the first set of simulations we want to analyze the behaviour of the cell over homogeneous soft and stiff substrates, respectively, in order to point out the main differences between the two. Thus, we have set $\mu_{\text{substrate}} = 3 \times 10^9$ Pa-s/m and an external attractant source is introduced at $\theta = 0$. The simulations cover a period of 600 s. The main quantitative results have been reported in table 2.

For the soft substrate, the cell is not able to adhere and pulses on place by protruding and contracting radially since $E_\alpha = E_\theta$ and an isotropic behaviour is observed (equation (12)) (available at stacks.iop.org/PB/12/026008/mmedia/movie 1). As the processes of polymerization and depolymerization of the actin filaments are responsible for the polarization of the cell, it is interesting to analyze the arrangement of the streamlines of the principal stresses, which provide an accurate picture of the load transfer inside the cell during migration and of the ability of the cell to maintain the necessary asymmetric distribution of the filaments to move forward (available at stacks.iop.org/PB/12/026008/mmedia/movie 1). In the specific case of a homogeneous soft substrate, the streamlines are radially oriented during both the protrusion (figure 3(a)) and contraction (figure 3(b)) phases, which reflects the absence of polarization leading to the inefficient pulsatile movement of the cell in place. The same distribution may be observed for the actin filaments in a rat embryonic fibroblast (REF52), which scarcely migrate over a soft substrate (figure 3(c)).

Table 1. Main geometrical and mechanical parameters of the model.

Parameter	Description	Value	Unit	Reference
r_{cell}	Cell radius	7.5	μm	[46, 47]
l_f	Distance cell centre—boundary of frontal adhesion region	4	μm	
l_r	Distance cell centre—boundary of rear adhesion region	4	μm	
Ω_{cell}	Initial cell area	176.6	μm^2	
Ω_f	Initial frontal adhesion region area	31	μm^2	
Ω_r	Initial rear adhesion region area	31	μm^2	
E_α	Cell Young modulus on soft substrate	10^3 (stiff) 10^4 (soft)	Pa	Deduced from equation (2)
E_θ	Cell Young modulus on stiff substrate	10^4	Pa	[44]
$\nu_{\theta\alpha}$	Cytoplasm Poisson ratio	0.4		
$\nu_{\alpha\theta}$	Cytoplasm Poisson ratio	0.4		
$G_{\theta\alpha}$	Shear modulus	384 (soft regions) 3846 (stiff regions)		
ρ	Cell density	1000	kg m^{-3}	[45]
e_{a0}	Amplitude of the active strain	0.8		
T	Migration period	60	s	
μ_{adh}	Cell friction coefficient	10^8	Pa-s/m	
	Substrate dimensions	70	μm	
$\mu_{substrate}$	Substrate friction coefficient	3×10^9	Pa-s/m	
x_0	Horizontal coordinate defining the boundary between the stiff and the soft substrate	20	μm	
$x_{stiff,1}$	x-coordinate of the centre for circular region 1	40	μm	
$x_{stiff,2}$	x-coordinate of the centre for circular region 2	20	μm	
$x_{stiff,3}$	x-coordinate of the centre for circular region 3	40	μm	
$x_{stiff,4}$	x-coordinate of the centre for circular region 4	0	μm	
$x_{stiff,5}$	x-coordinate of the centre for circular region 5	0	μm	
$y_{stiff,1}$	y-coordinate of the centre for circular region 1	0	μm	
$y_{stiff,2}$	y-coordinate of the centre for circular region 2	25	μm	
$y_{stiff,3}$	y-coordinate of the centre for circular region 3	50	μm	
$y_{stiff,4}$	y-coordinate of the centre for circular region 4	50	μm	
$y_{stiff,5}$	y-coordinate of the centre for circular region 5	0	μm	
r_{stiff}	Radius of the stiff circular regions	10	μm	

From a quantitative point of view, the average stresses developed inside the cell are equal to 0.03 μPa and 0.023 μPa respectively during protrusion and contraction. Thus, the cell only migrates over 2.7 μm (figure 4(a)) and this is mostly due to the inertial and viscous effects rather than to the active strain–adhesion forces machinery. The average velocity of the cell centre of inertia is equal to 0.011 μm s^{-1} and 0.007 μm s^{-1} during the protrusion and contraction phases respectively (figure 4(c)).

For the stiff substrate, no additional viscous force is applied and the cell is able to develop normal adhesion forces. Furthermore, according to equation (12), the mechanical behaviour is anisotropic which leads to an asymmetric strain in the direction of migration. During the protrusion phase, the streamlines of the principal stresses are still radially oriented, but more elongated at the leading edge in the direction of migration ($\theta = 0$) so that the cell is able to polarize and to efficiently migrate (figure 3(d), available at stacks.iop. org/PB/12/026008/mmedia/movie 2). A similar arrangement is found for a REF52 migrating over a

stiff substrate. In this case the actin filaments are oriented straight in the direction of migration, showing a very sharp polarity (figure 3(f)). During the contraction phase, the stresses are rather mixed up, but it is possible to observe a contraction at the rear edge, which allows the cell to pull its body forward (figure 3(e)). Then, the cell migrates over the substrate for 38 μm (figure 4(b)) with an average speed of about 0.12 μm s^{-1} and 0.08 μm s^{-1} respectively during protrusion and contraction (figure 4(d)) and generates higher average stresses compared to the previous case (0.08 μPa and 0.038 μPa during protrusion and contraction, respectively).
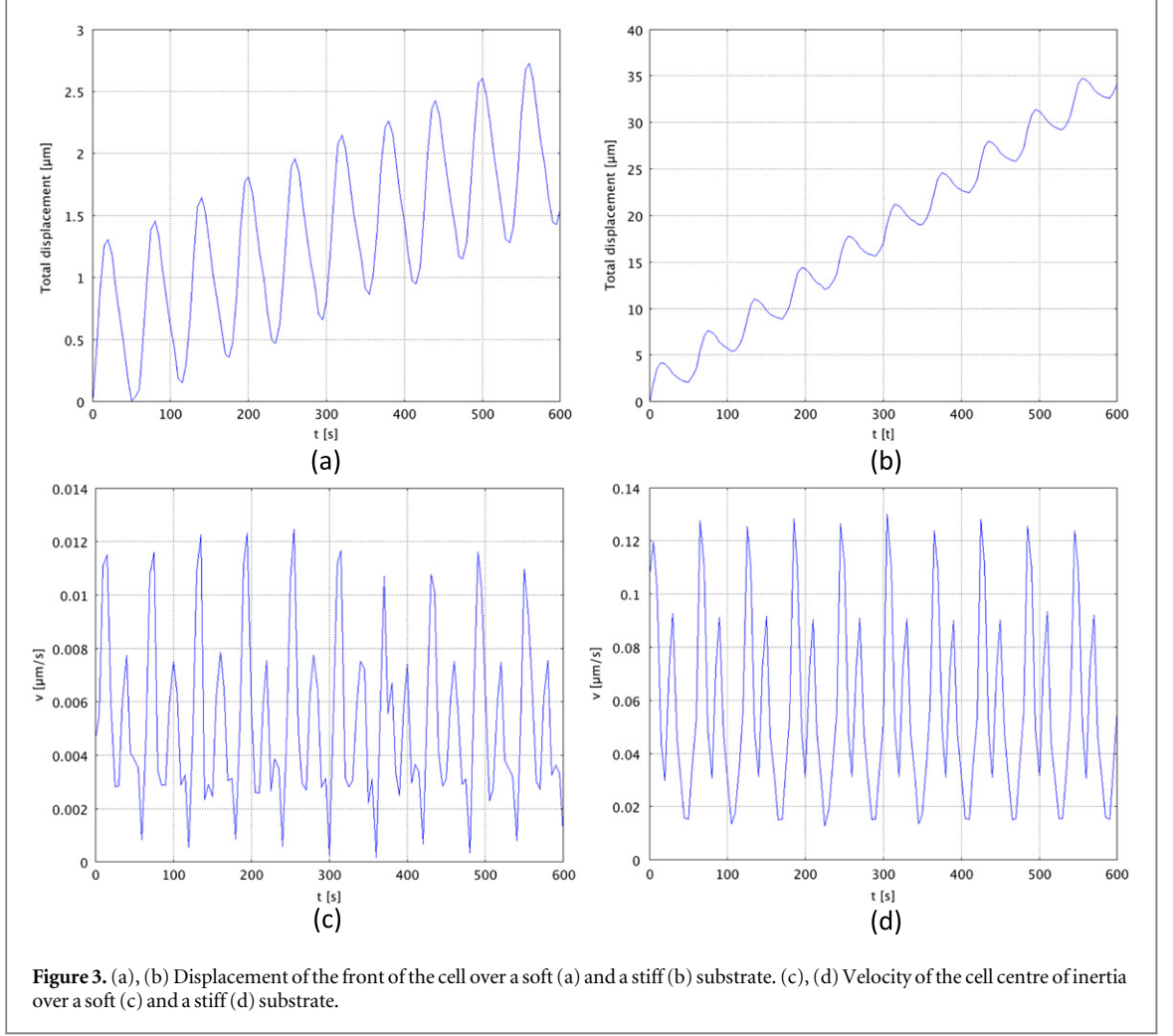
3.2. From stiff to soft substrate

For the second series of simulations we have considered a substrate made of both a stiff and a soft region. Three simulations have been run as described in the following.

First, we have kept attractive source at $\theta = 0$ (available at stacks.iop.org/PB/12/026008/mmedia/movie 3) and the boundary between the stiff and the

Table 2. Quantitative results for the numerical simulations.

	Time interval (s)	Direction of attractive source (°)	Displacement (μm)	Protrusion average speed (μm/s)	Contraction average speed (μm/s)	Protrusion average stress (μPa)	Contraction average stress (μPa)
Homogenous soft substrate	600	0	2.7	0.011	0.007	0.03	0.023
Homogeneous stiff substrate	600	0	38	0.12	0.08	0.08	0.038
Stiff to soft substrate	6000	0	33	0.11 (stiff)	0.07 (stiff)	0.05 (stiff)	0.028 (stiff)
				0.01 (soft)	0.006 (soft)	0.02 (soft)	0.001 (soft)
Stiff to soft substrate	6000	45	42	0.11 (stiff)	0.08 (stiff)	0.078 (stiff)	0.039 (stiff)
				0.01 (soft)	0.006 (soft)	0.035 (soft)	0.022 (soft)
Mapped Substrate	11000	45	54	0.01 (stiff)	0.07 (stiff)	0.08 (stiff)	0.04 (stiff)
				0.01 (soft)	0.006 (soft)	0.03 (soft)	0.02 (soft)

Figure 3. (a), (b) Displacement of the front of the cell over a soft (a) and a stiff (b) substrate. (c), (d) Velocity of the cell centre of inertia over a soft (c) and a stiff (d) substrate.
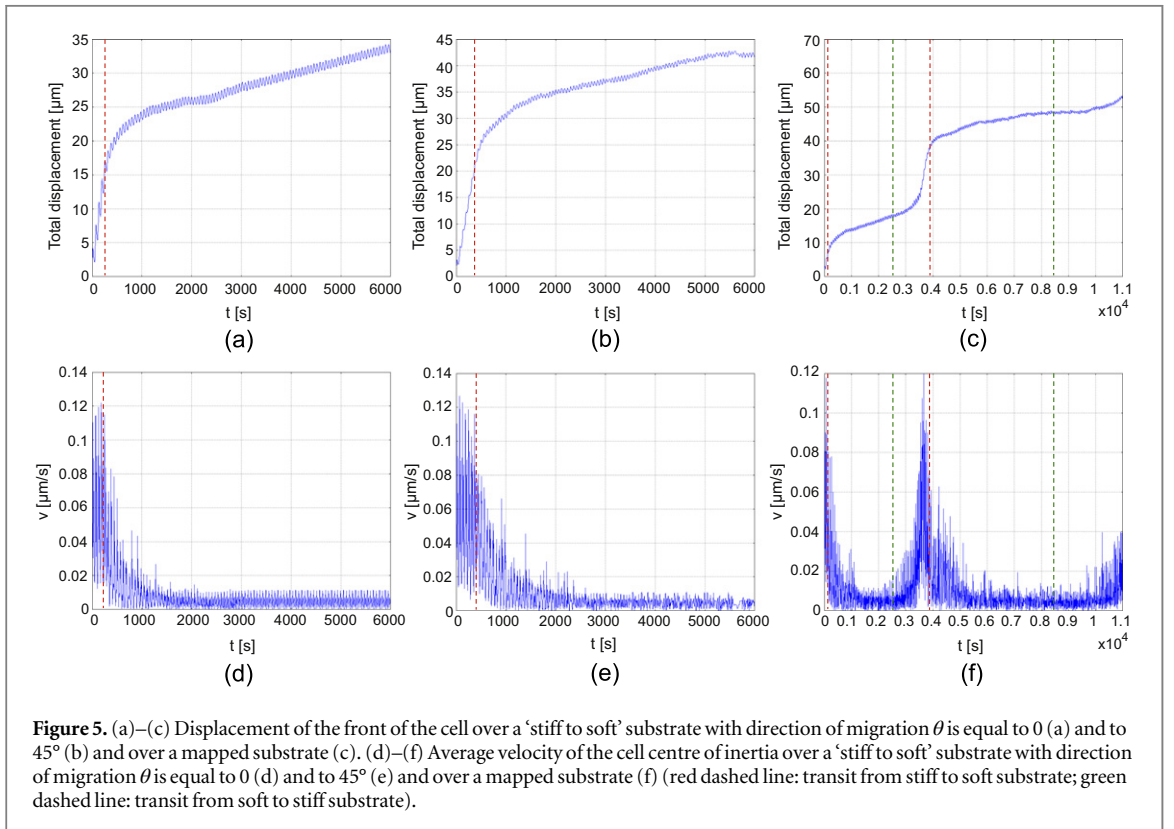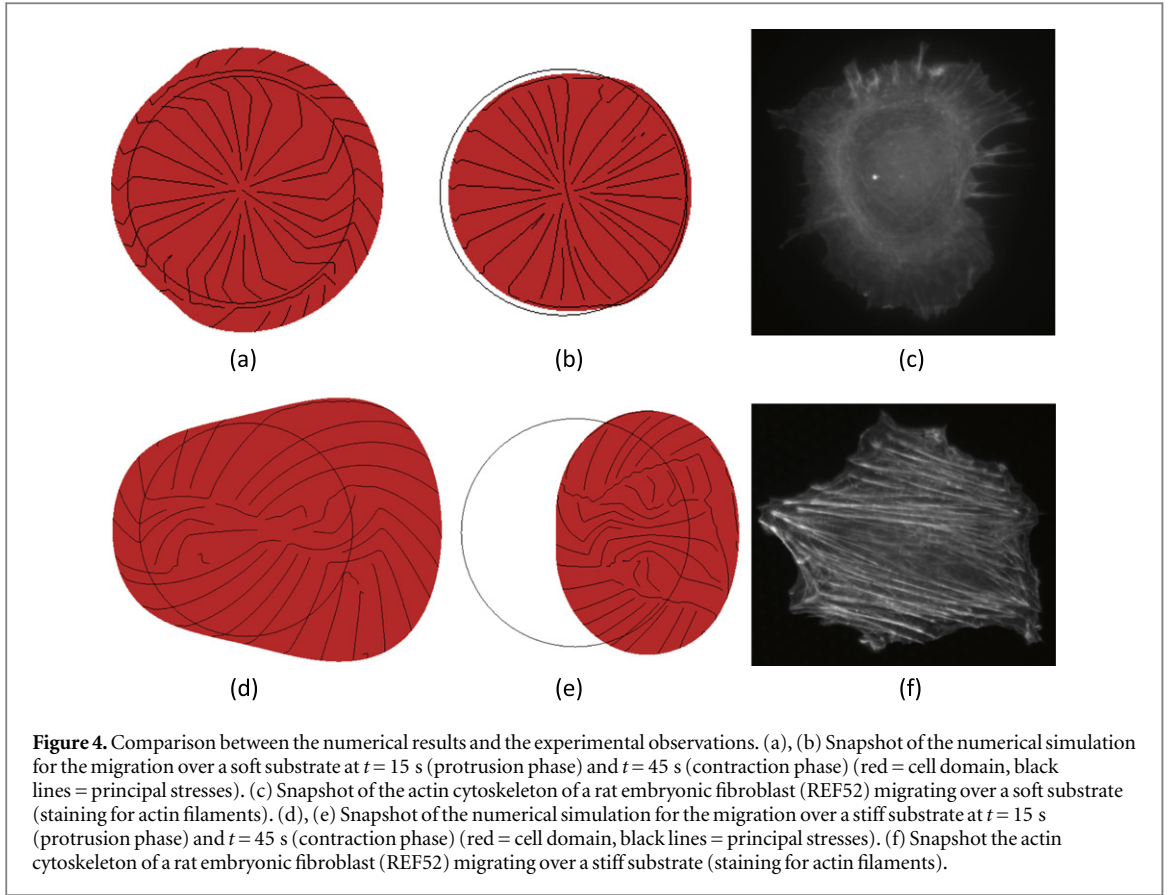
stiff region has been obtained via equation (1) for which x_0 has been fixed equal to 20 μm. In this case, the cell migrates over 33 μm during 6000 s (figure 5(a)), but a plateau is observed as soon as the cell comes into contact with the soft substrate. In fact, the average speed of the cell centre of migration switches from a value of around 0.08 μm s^{-1} to 0.008 μm s^{-1} around $t = 245$ s (figure 5(d)). In available at stacks.iop.org/PB/12/026008/mmedia/movie 3, it is possible to notice such a slowing down which also coincides with a reorganization of the principal stresses. In fact, over the stiff substrate, the streamlines of the principal stresses are radially oriented but elongated in the direction of migration leading to the polarization of the cell in the direction of migration, whereas over the soft substrate they are isotropically and radially arranged. Then, the cell efficiently moves over the stiff substrate since it is able to synchronize the active strains of protrusion and contraction with the adhesion forces, while it mainly pulses on place over the soft substrate.
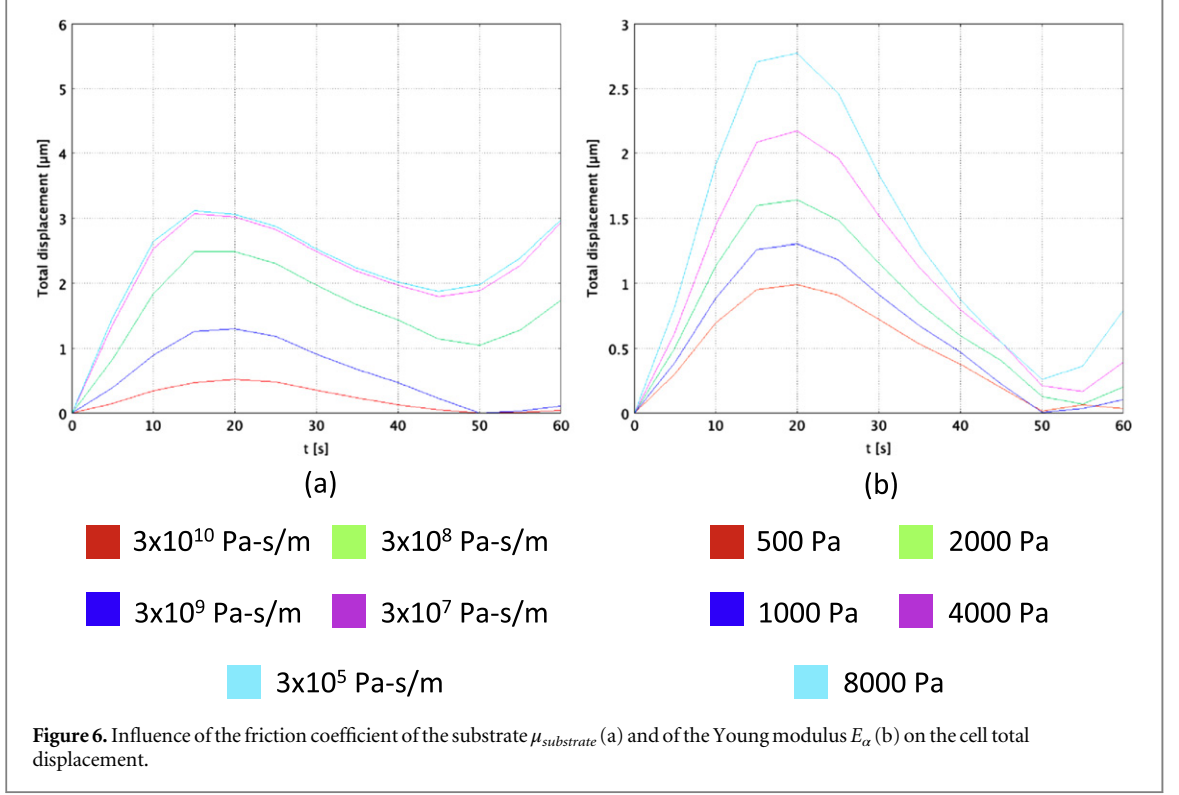
Second, the boundary between the stiff and the soft substrates has been kept the same, but the external source has been fixed at $\theta = 45°$ (available at stacks.iop. org/PB/12/026008/mmedia/movie 4). Here, the cell

covers a total distance of 42 μm over 6000 s and once again it is possible to notice both a plateau for the total displacement (figure 5(b)) and a change in the migration velocity as the cell reaches the soft substrate ($t = 375$ s) (figure 5(e)). In fact, the average speed decreases from 0.12 μm s^{-1} to 0.006 μm s^{-1}. One might wonder why the cell does not avoid contact with the soft substrate and look for an alternative path to reach the external source at 45° as it has been observed, for instance, in [2] where the cell moves along the boundary instead of crossing from the stiff to the soft substrate. Actually, in the present model the direction of migration is fixed and the cell does not have any notion of rotation as we proposed in [28] where it was able to detect an obstacle and change its orientation to circumvent it. Consequently, a change in direction may only occur if the balance of the momentum produces a rotation. This is the case here where the rear region of the cell is still on the stiff domain where the adhesion is higher, whereas the frontal edge is already on the soft domain. Thus, as the cell comes into contact with the soft region, it starts to slip and rotate so that the original direction of migration towards the external signal at $\theta = 45°$ is not maintained, but it becomes almost equal to 0°.

Figure 4. Comparison between the numerical results and the experimental observations. (a), (b) Snapshot of the numerical simulation for the migration over a soft substrate at $t = 15$ s (protrusion phase) and $t = 45$ s (contraction phase) (red = cell domain, black lines = principal stresses). (c) Snapshot of the actin cytoskeleton of a rat embryonic fibroblast (REF52) migrating over a soft substrate (staining for actin filaments). (d), (e) Snapshot of the numerical simulation for the migration over a stiff substrate at $t = 15$ s (protrusion phase) and $t = 45$ s (contraction phase) (red = cell domain, black lines = principal stresses). (f) Snapshot the actin cytoskeleton of a rat embryonic fibroblast (REF52) migrating over a stiff substrate (staining for actin filaments).

Figure 5. (a)–(c) Displacement of the front of the cell over a 'stiff to soft' substrate with direction of migration θ is equal to 0 (a) and to 45° (b) and over a mapped substrate (c). (d)–(f) Average velocity of the cell centre of inertia over a 'stiff to soft' substrate with direction of migration θ is equal to 0 (d) and to 45° (e) and over a mapped substrate (f) (red dashed line: transit from stiff to soft substrate; green dashed line: transit from soft to stiff substrate).

Third, the attractant is still place at $\theta = 45°$, but this time the substrate is made of circular stiff regions surrounded by soft regions (equation (2)), which leads to a mapped substrate (available at stacks.iop.org/PB/12/026008/mmedia/movie 5). The cell covers 54 μm over 11 000 s and two plateaux are observed corresponding

Figure 6. Influence of the friction coefficient of the substrate $\mu_{substrate}$ (a) and of the Young modulus E_α (b) on the cell total displacement.

to the passage of the cell over the soft regions ($t = 120$ s: 2190 s and $t = 3775$ s: 7500 s) (figure 5(c)). Similarly, the average speed of the cell centre of inertia is highest over the stiff regions ($0.1\,\mu$m s^{-1}) and lowest over the soft ones ($0.007\,\mu$m s^{-1}) (figure 5(f)).

3.3. Influence of the substrate stiffness and anisotropic Young modulus

For the last series of simulations, we have considered a homogenous soft substrate with an external source placed at $\theta = 0$ and we have let independently vary the friction coefficient of the substrate $\mu_{substrate}$ (equation (3)) and the Young modulus E_α (equation (12)). Then, we have evaluated the total displacement of the frontal edge of the cell over a first migration period (60 s) (figures 6(a) and (b)). On one hand, as $\mu_{substrate}$ decreases, the displacement increases since the cell is less inhibited by the additional viscous force exerted by the underneath substrate (figure 6 (a)). For a value of 3×10^5 Pa-s/m (light blue line in figure 6(a)), the cell covers approximately $3\,\mu$m during the first protrusion phase (from 0 to 15 s), which is close to the value found for the migration over a homogeneous stiff region of about $4\,\mu$m (see section 3.1). On the other hand, as E_α increases, the total displacement increases too (figure 6(b)). In fact, the higher E_α, the less the cell shows an anisotropic behaviour, which leads to a larger elongation in the direction of the attractant source $\theta = 0$. We found a minimal value of $1\,\mu$m for $E_\alpha = 500$ Pa (red line in figure 6(b)) and a maximal value of $2.7\,\mu$m for $E_\alpha = 8000$ Pa (light blue line in figure 6(b)).

4. Conclusions

We have proposed a 2D finite element model of cell migration over flat substrates including three main aspects of the process that are (i) durotaxis, (ii) cell polarity and (iii) cell anisotropy. The cell has been modelled as a continuum and a generalized Maxwell model with anisotropic elastic branch has been employed to describe the viscoelastic behaviour of the system. The cell is able to synchronize the active strains of protrusion and contraction with the adhesion forces with the underneath substrate, which is represented as a 2D square and may include both stiff and soft regions. The latter trigger a further viscous force inhibiting the cell progression. First, we have analyzed the cell behaviour over homogenous stiff and soft regions and we have observed a clear difference in terms of efficiency. In fact, over the soft substrate the cell is not able to adhere and is almost stuck in place, whereas over the stiff region it is able to normally migrate. The numerical results have also been qualitatively compared to specific experimental images. Second, we have tested three different configurations: (i) a stiff-to-soft region with sharp boundary and external source placed at 0°, (ii) a stiff-to-soft region with sharp boundary and attractive source placed at 45° and (iii) circular stiff regions surrounded by a soft matrix and external source placed at 45°. We have quantitatively evaluated the total cover distance, the migration velocity, and the average stress inside the cell. Finally, we have investigated the influence of both the substrate stiffness and the anisotropic Young modulus on the cell efficiency.

10

References

[1] Giannone G, Dubin-Thaler B J, Döbereiner H-G, Kieffer N, Bresnick A R and Sheetz M P 2004 Periodic lamellipodial contractions correlate with rearward actin waves *Cell* **116** 431–43

[2] Lo C M, Wang H B, Dembo M and Wang Y L 2000 Cell movement is guided by the rigidity of the substrate *Biophys. J.* **79** 144–52

[3] Engler A J, Sen S, Sweeney H L and Discher D E 2006 Matrix elasticity directs stem cell lineage specification *Cell* **126** 677–89

[4] Bischofs I B and Schwarz U S 2003 Cell organization in soft media due to active mechanosensing *PNAS* **100** 9274–9

[5] Balaban N Q, Schwarz U S, Riveline D, Goichberg P, Tzur G, Sabanay I, Mahalu D, Safran S, Bershadsky A, Addadi L and Geiger B 2001 Force and focal adhesion assembly: a close relationship studied using elastic micropatterned substrates *Nat. Cell Biol.* **3** 466–72

[6] Tan J L, Tien J, Pirone D M, Gray D S, Bhadriraju K and Chen C S 2003 Cells lying on a bed of microneedles: an approach to isolate mechanical force *Proc. Natl Acad. Sci. USA* **100** 1484–9

[7] Nicolas A, Geiger B and Safran S A 2004 Cell mechanosensitivity controls the anisotropy of focal adhesions *PNAS* **101** 12520–5

[8] Shemesh T, Geiger B, Bershadsky A D and Kozlov M M 2005 Focal adhesions as mechanosensors: a physical mechanism *PNAS* **102** 12383–8

[9] Glogauer M, Arora P, Yao G, Sokholov I, Ferrier J and McCulloch C A 1997 Calcium ions and tyrosine phosphorylation interact coordinately with actin to regulate cytoprotective responses to stretching *J. Cell. Sci.* **110** 11–21 (Pt 1)

[10] Hayakawa K, Tatsumi H and Sokabe M 2008 Actin stress fibers transmit and focus force to activate mechanosensitive channels *J. Cell. Sci.* **121** 496–503

[11] Mitrossilis D, Fouchard J, Guiroy A, Desprat N, Rodriguez N, Fabry B and Asnacios A 2009 Single-cell response to stiffness exhibits muscle-like behavior *PNAS* **106** 18243–8

[12] Lam W A, Chaudhuri O, Crow A, Webster K D, Li T-D, Kita A, Huang J and Fletcher D A 2011 Mechanics and contraction dynamics of single platelets and implications for clot stiffening *Nat. Mater.* **10** 61–6

[13] Walcott S and Sun S X 2010 A mechanical model of actin stress fiber formation and substrate elasticity sensing in adherent cells *Proc. Natl Acad. Sci. USA* **107** 7757–62

[14] Kobayashi T and Sokabe M 2010 Sensing substrate rigidity by mechanosensitive ion channels with stress fibers and focal adhesions *Curr. Opin. Cell Biol.* **22** 669–76

[15] Iskratsch T, Wolfenson H and Sheetz M P 2014 Appreciating force and shape—The rise of mechanotransduction in cell biology *Nat. Rev. Mol. Cell Biol.* **15** 825–33

[16] Ladoux B and Nicolas A 2012 Physically based principles of cell adhesion mechanosensitivity in tissues *Rep. Prog. Phys.* **75** 116601

[17] Saez A, Ghibaudo M, Buguin A, Silberzan P and Ladoux B 2007 Rigidity-driven growth and migration of epithelial cells on microstructured anisotropic substrates *PNAS* **104** 8281–6

[18] Trichet L, Digabel J L, Hawkins R J, Vedula S R K, Gupta M, Ribrault C, Hersen P, Voituriez R and Ladoux B 2012 Evidence of a large-scale mechanosensing mechanism for cellular adaptation to substrate stiffness *PNAS* **109** 6933–8

[19] Raab M, Swift J, Dingal P C D P, Shah P, Shin J-W and Discher D E 2012 Crawling from soft to stiff matrix polarizes the cytoskeleton and phosphoregulates myosin-II heavy chain *J. Cell Biol.* **199** 669–83

[20] Zemel A and Safran S A 2007 Active self-polarization of contractile cells in asymmetrically shaped domains *Phys. Rev. E* **76** 021905

[21] De R, Zemel A and Safran S A 2007 Dynamics of cell orientation *Nat. Phys.* **3** 655–9

[22] Mitrossilis D, Fouchard J, Pereira D, Postic F, Richert A, Saint-Jean M and Asnacios A 2010 Real-time single-cell response to stiffness *PNAS* **107** 16518–23

[23] Schwarz U S and Safran S A 2013 Physics of adherent cells *Rev. Mod. Phys.* **85** 1327–81

[24] Moreo P, García-Aznar J M and Doblaré M 2008 Modeling mechanosensing and its effect on the migration and proliferation of adherent cells *Acta Biomater.* **4** 613–21

[25] Dokukina I V and Gracheva M E 2010 A model of fibroblast motility on substrates with different rigidities *Biophys. J.* **98** 2794–803

[26] Harland B, Walcott S and Sun S X 2011 Adhesion dynamics and durotaxis in migrating cells *Phys. Biol.* **8** 015011

[27] Stefanoni F, Ventre M, Mollica F and Netti P A 2011 A numerical model for durotaxis *J. Theor. Biol.* **280** 150–8

[28] Allena R and Aubry D 2012 'Run-and-tumble' or 'look-and-run'? A mechanical model to explore the behavior of a migrating amoeboid cell *J. Theor. Biol.* **306** 15–31

[29] Aubry D, Thiam H, Piel M and Allena R 2015 A computational mechanics approach to assess the link between cell morphology and forces during confined migration *Biomech. Model. Mechanobiol.* **4** 143–57

[30] Allena R 2013 Cell migration with multiple pseudopodia: temporal and spatial sensing models *Bull. Math. Biol.* **75** 288–316

[31] Gracheva M E and Othmer H G 2004 A continuum model of motility in ameboid cells *Bull. Math. Biol.* **66** 167–93

[32] Felder S and Elson E L 1990 Mechanics of fibroblast locomotion: quantitative analysis of forces and motions at the leading lamellas of fibroblasts *J. Cell Biol.* **111** 2513–26

[33] Schaub S, Bohnet S, Laurent V M, Meister J-J and Verkhovsky A B 2007 Comparative maps of motion and assembly of filamentous actin and myosin II in migrating cells *Mol. Biol. Cell* **18** 3723–32

[34] Mogilner A 2009 Mathematics of cell motility: have we got its number? *J. Math. Biol.* **58** 105–34

[35] Holzapfel G A 2000 *Nonlinear Solid Mechanics: A Continuum Approach for Engineering* (Chichester: Wiley)

[36] Taber L A 2004 *Nonlinear Theory of Elasticity: Applications in Biomechanics* (Singapore: World Scientific)

[37] Ambrosi D and Pezzuto S 2011 Active stress versus active strain in mechanobiology: constitutive issues *J. Elast.* **107** 199–212

[38] Taber L A and Perucchio R 2000 Modeling heart development *J. Elast.* **61** 165–97

[39] Cherubini C, Filippi S, Nardinocchi P and Teresi L 2008 An electromechanical model of cardiac tissue: constitutive issues and electrophysiological effects *Prog. Biophys. Mol. Biol.* **97** 562–73

[40] Muñoz J J, Barrett K and Miodownik M 2007 A deformation gradient decomposition method for the analysis of the mechanics of morphogenesis *J. Biomech.* **40** 1372–80

[41] Conte V, Muñoz J J and Miodownik M 2008 A 3D finite element model of ventral furrow invagination in the Drosophila melanogaster embryo *J. Mech. Behav. Biomed. Mater.* **1** 188–98

[42] Phillipson M, Heit B, Colarusso P, Liu L, Ballantyne C M and Kubes P 2006 Intraluminal crawling of neutrophils to emigration sites: a molecularly distinct process from adhesion in the recruitment cascade *J. Exp. Med.* **203** 2569–75

[43] Sakamoto Y, Prudhomme S and Zaman M H 2011 Viscoelastic gel-strip model for the simulation of migrating cells *Ann. Biomed. Eng.* **39** 2735–49

[44] Laurent V M, Kasas S, Yersin A, Schäffer T E, Catsicas S, Dietler G, Verkhovsky A B and Meister J-J 2005 Gradient of rigidity in the lamellipodia of migrating cells revealed by atomic force microscopy *Biophys. J.* **89** 667–75

[45] Fukui Y, Uyeda T Q P, Kitayama C and Inoué S 2000 How well can an amoeba climb? *PNAS* **97** 10020–5

[46] Ronot X, Doisy A and Tracqui P 2000 Quantitative study of dynamic behavior of cell monolayers during *in vitro* wound healing by optical flow analysis *Cytometry* **41** 19–30

[47] Ngalim S H, Magenau A, Zhu Y, Tønnesen L, Fairjones Z, Gooding J J, Böcking T and Gaus K 2013 Creating adhesive and soluble gradients for imaging cell migration with fluorescence microscopy *J. Vis. Exp.* **74** 50310